Neuron
Article

Rhythmic Fluctuations in Evidence Accumulation during Decision Making in the Human Brain

Valentin Wyart,[1,2,*] Vincent de Gardelle,[1] Jacqueline Scholl,[1] and Christopher Summerfield[1]
[1]Department of Experimental Psychology, University of Oxford, South Parks Road, Oxford OX1 3UD, UK
[2]Laboratoire de Neurosciences Cognitives, Département d'Etudes Cognitives, Ecole Normale Supérieure, 29 rue d'Ulm, 75005 Paris, France
*Correspondence: valentin.wyart@ens.fr
http://dx.doi.org/10.1016/j.neuron.2012.09.015

SUMMARY

Categorical choices are preceded by the accumulation of sensory evidence in favor of one action or another. Current models describe evidence accumulation as a continuous process occurring at a constant rate, but this view is inconsistent with accounts of a psychological refractory period during sequential information processing. During multisample perceptual categorization, we found that the neural encoding of momentary evidence in human electrical brain signals and its subsequent impact on choice fluctuated rhythmically according to the phase of ongoing parietal delta oscillations (1–3 Hz). By contrast, lateralized beta-band power (10–30 Hz) overlying human motor cortex encoded the integrated evidence as a response preparation signal. These findings draw a clear distinction between central and motor stages of perceptual decision making, with successive samples of sensory evidence competing to pass through a serial processing bottleneck before being mapped onto action.

INTRODUCTION

Integrating multiple samples of evidence helps optimize behavior by allowing the true state of the environment to be estimated more precisely (Wald and Wolfowitz, 1949; Bogacz et al., 2006). Current decision-theoretic models assume that momentary evidence is accumulated at a constant rate in the form of a decision variable, a quantity that maps the integrated evidence onto an appropriate action (Link, 1975; Ratcliff and Smith, 2004). These linear integration models have drawn support from neurophysiological recordings in the nonhuman primate that have demonstrated a gradual buildup of neuronal firing rates in the lateral intraparietal cortex during evidence accumulation (Shadlen and Newsome, 2001; Roitman and Shadlen, 2002; Gold and Shadlen, 2003, 2007). This work has led to the prevailing view that sensory information is converted fluidly and continuously into action, with the encoding of momentary evidence and its integration in sensorimotor cortex forming an indivisible precursor to choice.

However, the notion that sensory evidence is integrated linearly and continuously is at odds with a rich psychological literature describing how human perception is limited by a central processing bottleneck (Marois and Ivanoff, 2005), giving rise to a psychological refractory period of a few hundreds of milliseconds during which relevant sensory information is perceived as lagging (Pashler, 1984) or even missed (Raymond et al., 1992). One intuitive explanation for these refractory periods is that humans are constrained to sample the environment discretely in rhythmic frames lasting up to hundreds of milliseconds (VanRullen and Koch, 2003), thereby allocating processing resources to incoming sensory information depending on its position within the sampling cycle (Busch and VanRullen, 2010). In accordance with this rhythmic sampling view, an emerging neurophysiological framework proposes that slow cortical oscillations in the delta band (1–3 Hz) can serve as instruments of attentional selection by modulating rhythmically the gain of information processing (Lakatos et al., 2008; Schroeder and Lakatos, 2009). However, these temporally structured slow fluctuations in neural excitability have only been observed in early sensory cortex and at frequencies that match the presentation rate of relevant stimuli, making it unclear whether they reflect a temporal constraint on sequential information processing.

One central prediction arising from this rhythmic account of information processing is that humans should exhibit slow rhythmic fluctuations in their rate of evidence accumulation during decision making—in other words, that samples of evidence that strongly influence choice should be succeeded by a refractory period during which new samples have a weaker impact on the same choice. Critically, this push-pull pattern of decision "weighting" should follow the phase of cortical delta oscillations. Here we tested these predictions by recording human electroencephalogram (EEG) signals during a perceptual categorization task that required the integration of multiple samples of evidence over time. We found that the neural encoding of individual samples of evidence and their decision weight on a categorical choice occurring several hundreds of milliseconds later fluctuated rhythmically according to the phase of delta oscillations overlying human parietal cortex.

RESULTS

We recorded scalp EEG signals from 15 human participants who viewed a rapid stream of eight oriented Gabor patterns presented at a rate of 4 Hz (Figure 1A). Following each stream, participants reported whether, on average, the tilt of the eight elements fell closer to the cardinal or diagonal axes. We defined

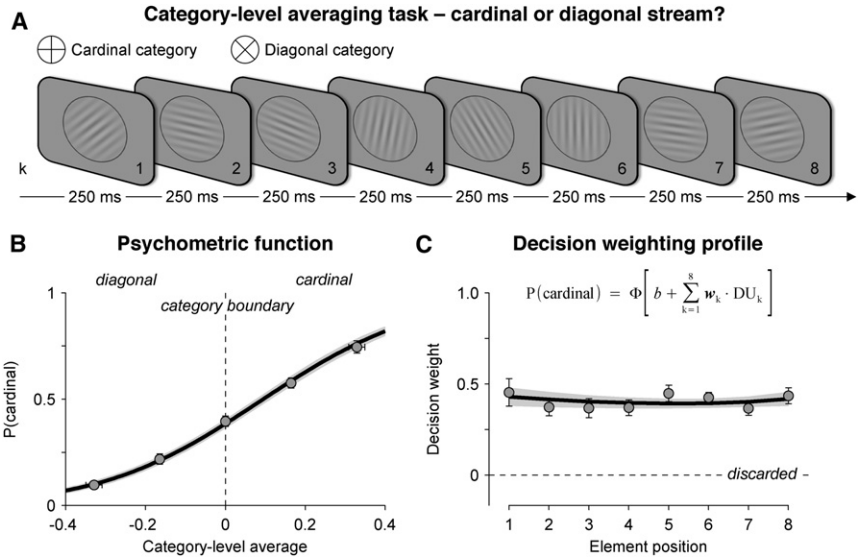

Figure 1. Experimental Design and Behavior

(A) Category-level averaging task. Rapid visual streams of eight oriented Gabor patterns were presented at a stimulation rate of 4 Hz. Participants reported whether, on average, the tilt of the eight elements fell closer to the cardinal or diagonal axis.

(B) Psychometric function relating the category-level average (x axis), divided into five equally spaced levels, to the probability of judging the stream as being cardinal (y axis). Dots and attached error bars indicate participants' data (mean ± SEM). The black line (and its shaded error bar indicating SEM) indicates the best-fitting cumulative normal function estimated via a logistic regression of choice against the category-level average.

(C) Decision weighting profile across the eight elements. Individual decision weights are estimated using a multivariate logistic regression of choice against a linear combination of the eight decision updates (inset equation). Dots and attached error bars indicate participants' data. The black line (and its shaded error bar) indicates the best-fitting exponential profile. Same conventions as in (B).

two parametric quantities indexing two types of information provided by each element on each trial: (1) the *perceptual update* (or PU_k), corresponding to the absolute difference in tilt between a given element k and the previous element k−1, and (2) the *decision update* (or DU_k), corresponding to the amount of categorical evidence provided by element k.

In other words, perceptual updates reflect how much each new element differs visually from the previous one—i.e., the successive visual transients occurring at the onset of each new element—whereas decision updates reflect how much each new element differs from the decision criterion—i.e., the incremental quantity that the internal decision variable should be updated with (see Figure S1 available online). Critically, the use of a cardinal/diagonal decision axis ensured that PU_k and DU_k were uncorrelated across trials—i.e., two elements could give rise to identical perceptual updates but different decision updates (see Experimental Procedures; Figure S1). Perceptual updates are irrelevant to performing the task, whereas decision updates correspond to the quantity that subjects should integrate over time: the sum of the eight decision updates, each signed with its corresponding category. Finally, we ensured that successive decision updates were not correlated across trials by sampling them randomly from independent uniform distributions (Figure S1); this feature allowed us to regress individual decision weights with the highest statistical power.

Categorization accuracy was titrated for each participant prior to the experiment by adjusting the average categorical evidence available at the end of the trial over five evenly spaced levels (Figure 1B). We then estimated the *decision weight* (or w_k) associated with each element k, defined as its multiplicative contribution to the subsequent choice. We calculated these weights across trials via a multivariate parametric regression of choice on the basis of a linear combination of the eight decision updates:

$$P(\text{cardinal}) = \Phi\left[b + \sum_{k=1}^{8} w_k \cdot DU_k\right],$$

where P(cardinal) corresponds to the probability of judging the stream as cardinal, Φ to the cumulative normal function, and *b* to an additive *response bias* toward one of the two categories. We found that decision weights were all positive (t test against zero, all $p < 0.001$) and statistically indistinguishable across successive elements (repeated-measures ANOVA, $F_{7,98} < 1$, $p > 0.5$), indicating that across trials, participants weighted the eight elements equally, irrespective of their position within the stream (Figure 1C).

We further tested whether successive elements contributed independently to the final choice—e.g., whether past decision updates did not influence the contribution of future elements to the final choice. We found that subjects indeed used the decision information provided by successive elements in an orthogonal fashion (Figure S1): for any given element, the magnitude of previous and next decision updates did not influence the contribution of the current element to choice (see Supplemental Information).

Neural Encoding of Perceptual and Decision Updates

We began by identifying the neural correlates of perceptual and decision updates by regressing single-trial EEG signals, filtered at 1–16 Hz, against these two parametric quantities at successive time samples following the onset of each element. The resulting *encoding* time courses are not event-related potentials but estimates of the extent to which single-trial EEG signals encode PU_k and DU_k in a parametric fashion (see Experimental Procedures).

This analysis revealed spatially and temporally distinct correlates of perceptual and decision updates (Figure 2). The

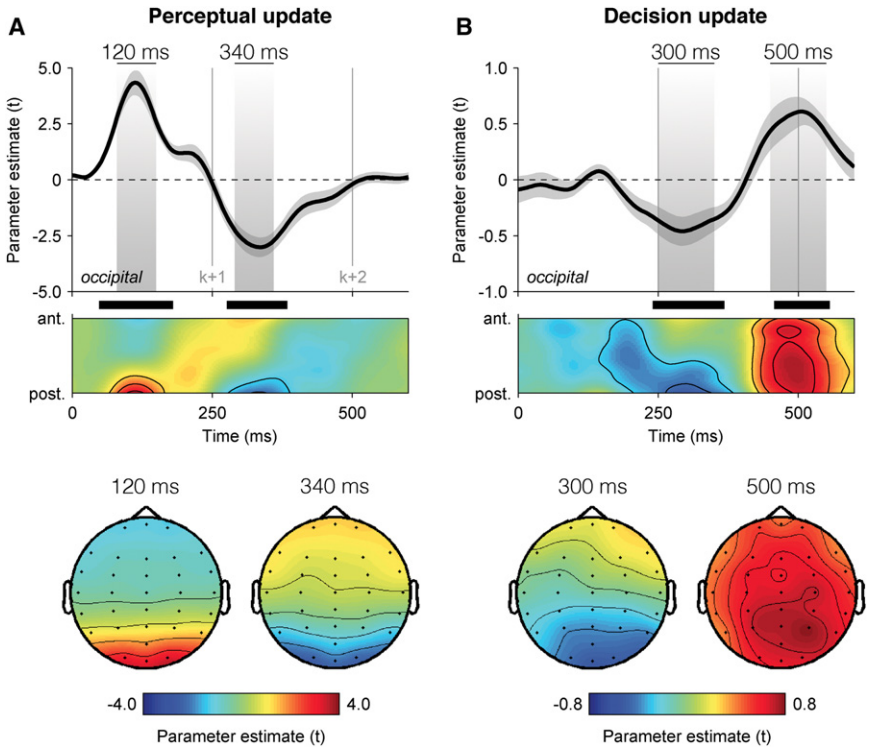

Figure 2. Dissociable Neural Encoding of Perceptual and Decision Updates

(A) Neural encoding of perceptual update PU_k in EEG signals, expressed as parameter estimate in t units. Upper panel: encoding time course at occipital electrodes (above) and following a spatial anteroposterior gradient from electrode FPz to electrode Oz (below). Shaded areas highlight positive and negative components peaking, respectively, at 120 ms (left) and 340 ms (right) following element k. Lower panel: encoding scalp topographies at 120 ms (left) and 340 ms (right) following element k. Shaded error bars indicate SEM. Thick black lines indicate cluster-level significance at $p < 0.001$.

(B) Neural encoding of decision update DU_k in EEG signals. Upper panel: encoding time course at occipital electrodes (above) and following the anteroposterior gradient (below). Shaded areas highlight negative and positive components peaking, respectively, at 300 ms and 500 ms following element k. Lower panel: encoding scalp topographies at 300 ms (left) and 500 ms (right) following element k. Same conventions as in (A).

encoding of PU_k peaked at 120 ms following the onset of element k at occipital electrodes (t test against zero, peak $t_{14} = 8.2$, cluster-level $p < 0.001$), whereas the encoding of DU_k showed a negative component at 300 ms followed by a positive one at 500 ms, the latter being more distributed across the scalp but peaking at parietal electrodes (peak $t_{14} = 5.6$, cluster-level $p < 0.001$). In other words, elements were processed perceptually before 100 ms, and converted into decision-relevant signals by 250 ms.

The fact that the encoding of each perceptual/decision update was not completed by 250 ms—i.e., at the onset of the next element—suggests that the encoding of successive updates was partially overlapping (Figure S2). To confirm this, we entered simultaneously previous, current, and next perceptual/decision updates as multiple regressors of single-trial EEG signals (see Supplemental Information) and observed overlapping encoding time courses that were indistinguishable from those obtained via univariate regression. Importantly, this finding demonstrates that the neural encoding of element k following the onset of element k+1 is not contaminated by the neural encoding of element k+1.

Neural Decoding of Individual Decision Weights

Subsequently, we estimated the extent to which the neural encoding of decision updates for each element k predicted the decision weight w_k assigned to that element in the eventual choice. This *decoding* analysis measures the subjective choice-predictive information available in neural encoding signals, over and above the objective categorical information provided by each element. Capitalizing on trial-to-trial variability in the encoding of DU_k, we tested whether encoding residuals—trial-to-trial fluctuations in EEG signals unexplained by DU_k—covaried with w_k across trials (see Experimental Procedures). We calculated the strength $w_{k,t}$ of this psychophysiological interaction at successive time points following each element k via a multivariate parametric regression for which the interaction between each decision update DU_k and the corresponding encoding residuals $r_{k,t}$ at time t was modeled as an additional predictor of choice:

$$P(\text{cardinal}) = \Phi\left[b + \sum_{k=1}^{8} w_k \cdot DU_k + \sum_{k=1}^{8} w_{k,t} \cdot DU_k \times r_{k,t}\right].$$

The time course of this psychophysiological modulation $w_{k,t}$ (Figure 3A) matched that observed for the neural encoding of DU_k, with a negative component at 300 ms followed by a positive one at 500 ms at parietal electrodes (t test against zero, peak $t_{14} = 7.2$, cluster-level $p < 0.001$). In other words, elements for which the neural encoding of DU_k was stronger were overweighted in the subsequent choice, whereas elements for which the neural encoding of DU_k was weaker were underweighted (Figure 3B).

Our main hypothesis was that the weighting of momentary evidence during its accumulation would fluctuate rhythmically. We thus assessed whether the strength of the neural encoding of DU_k also influenced the decision weights associated with temporally adjacent elements in the stream (Figures 3C and S3). Consistent with a fluctuating gain of evidence accumulation, the neural encoding of DU_k was inversely related to the decision weight w_{k+1} associated with the subsequent element. In other words, a stronger neural encoding of DU_k predicted not only the overweighting of the current element but also the underweighting of the next element presented 250 ms later. This

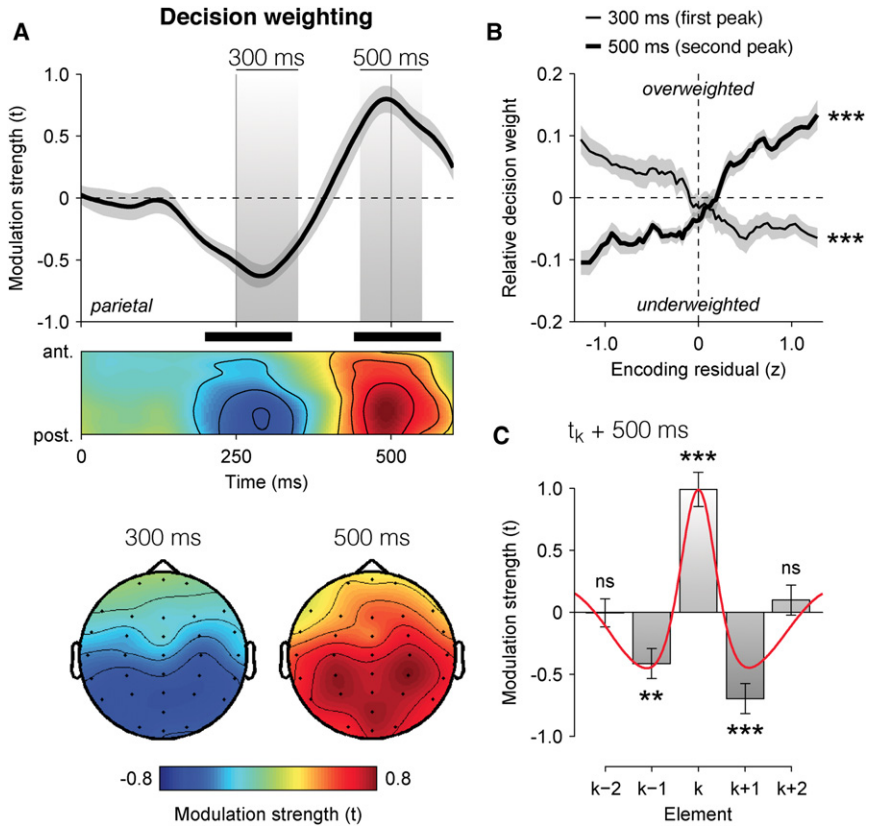

Figure 3. Neural Decoding of Individual Decision Weights

(A) Neural decoding of multiplicative decision weighting in EEG signals, expressed as modulation strength in t units. Upper panel: decision weight decoding time course at parietal electrodes (above) and following the anteroposterior gradient (below). Shaded areas highlight negative and positive components peaking, respectively, at 300 ms and 500 ms following element k. Lower panel: decoding scalp topographies at 300 ms (left) and 500 ms (right) following element k. Shaded error bars indicate SEM. Thick black bars indicate cluster-level significance at $p < 0.001$.

(B) Relationship between encoding residuals at 300 ms (thin) and 500 ms (thick) following element k at parietal electrodes, binned in 64 overlapping quartiles, and the relative (mean-subtracted) decision weight w_k. Shaded error bars indicate SEM.

(C) Neural decoding of successive decision weights assigned to elements k−1 and k+1 at 500 ms following element k. Error bars indicate SEM. Significant modulation at $^{**}p < 0.01$ and $^{***}p < 0.001$. The red line indicates the raw autocorrelation profile of parietal EEG signals. ns, nonsignificant modulation.

inverse relationship was maximal at parietal electrodes at 500 ms following element k (t test against zero, $t_{14} = -6.0$, $p < 0.001$). This "push-pull" pattern of decision weighting was also significant for the previous element k−1 ($t_{14} = -3.8$, $p = 0.001$) but not for further elements k−2 and k+2 (both $p > 0.1$), indicating that this competitive interaction between decision weights was focal in time—i.e., strongest for immediately adjacent elements in the stream.

Slow Rhythmic Fluctuations in Neural Encoding and Decision Weighting

If momentary evidence is sampled in a rhythmic fashion, then the neural encoding of DU_k and its decision weight w_k should depend on the phase of slow cortical oscillations, possibly in the delta band (1–3 Hz), where the period matches the refractory pattern of decision weighting observed across successive elements (Figure 3C).

We thus assessed whether the phase of EEG oscillations between 1 and 16 Hz influenced the neural encoding of DU_k (see Experimental Procedures). Sorting single trials according to their phase at 2 Hz measured at 500 ms following element k at parietal electrodes (Figures 4A and S4), we observed that the neural encoding of DU_k was stronger at the peak and weaker at the trough of the delta cycle at 2 Hz (Rayleigh test, $r_{14} = 0.47$, $p = 0.01$). Importantly, the decision weight w_k assigned to element k also depended on delta phase (Figure 4B), following the same phase relationship ($r_{14} = 0.90$, $p < 0.001$); in other words, the samples of evidence that fell at the preferred delta phase were encoded more strongly and overweighted in the subsequent choice. By contrast, those that fell in the opposite delta phase—typically the following element presented 250 ms later—were poorly encoded and underweighted in the same choice. This phasic modulation of decision weighting was significant for all elements (t test against zero, all $p < 0.05$), and did not interact with the position of element k (repeated-measures ANOVA, $F_{7,98} < 1$, $p > 0.5$) or with the amount of categorical evidence available at the end of the stream ($F_{2,28} < 1$, $p > 0.2$).

For completeness, we also assessed whether the phase of EEG oscillations between 1 and 16 Hz influenced the neural encoding of perceptual updates (Figures 4C and S4). As observed for DU_k, we found that the neural encoding of PU_k at 120 ms following element k at occipital electrodes covaried with delta phase at 2 Hz (Rayleigh test, $r_{14} = 0.69$, $p < 0.001$). However, in contrast to DU_k, the neural encoding of PU_k was strongest at the trough and weakest at the peak of the delta cycle, and also depended on theta phase at 8 Hz ($r_{14} = 0.45$, $p < 0.05$) following the same phase relationship, thereby matching previous observations (Busch and VanRullen, 2010; Stefanics et al., 2010).

To verify that this phasic effect at 2 Hz was not a consequence of our rhythmic presentation rate, we calculated steady-state spectral power and phase locking across trials between 1 and 16 Hz and found anticipated peaks at the stimulation frequency (4 Hz) and its higher harmonics, but no peak in the delta band (Figure 5A). Subtracting the average steady-state broadband response from the EEG data (Figure S5) before estimating delta phase did not change the observed pattern of results, either qualitatively or quantitatively. Slow fluctuations in decision

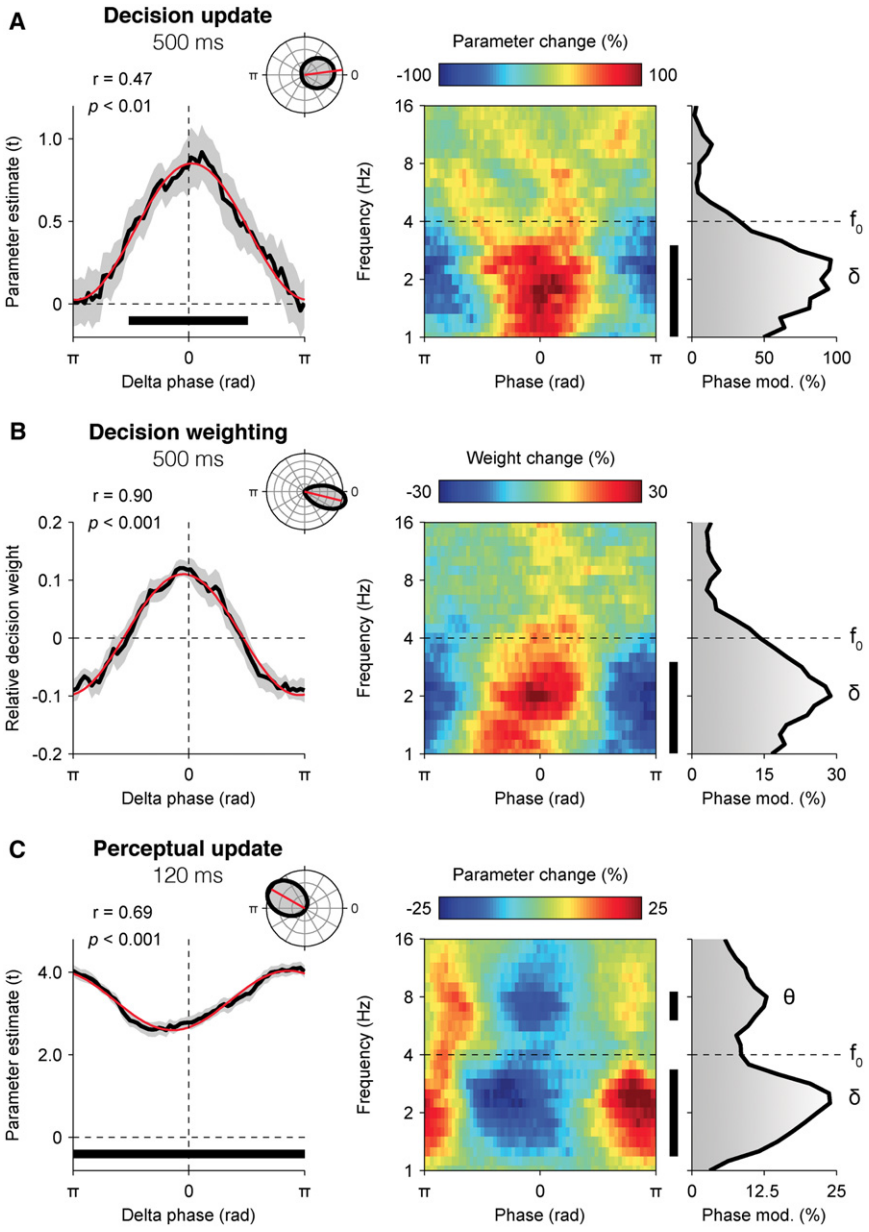

Figure 4. Slow Rhythmic Fluctuations in Neural Encoding and Decision Weighting

(A) Phase-dependent fluctuations in the neural encoding of decision updates at parietal electrodes. Left panel: relationship between delta phase and the encoding of decision update DU_k at 500 ms following element k at parietal electrodes. Inset: distribution of preferred phase across participants (0: peak; π: trough). Shaded error bars indicate SEM. The red sinusoid indicates the best fit. The thick black line indicates significant neural encoding at $p < 0.01$ (two-tailed). Right panel: relationship between the phase of EEG oscillations from 1 to 16 Hz and the neural encoding of decision update DU_k at 500 ms following element k at parietal electrodes. Phase modulation corresponds to the relative amplitude of the best sinusoidal fit. f_0 indicates stimulation frequency (4 Hz).

(B) Phase-dependent fluctuations in decision weight w_k at 500 ms following element k at parietal electrodes. Same conventions as in (A).

(C) Phase-dependent fluctuations in the neural encoding of perceptual update PU_k at 120 ms following element k at occipital electrodes. Same conventions as in (A).

weighting thus followed the phase of endogenous, non-phase-locked delta oscillations, not the phase of a fixed subharmonic of the stimulation frequency. Importantly, shuffling phase information across trials confirmed that this phasic modulation of decision weighting could not be due to the entrainment of EEG oscillations to the stimulation frequency; indeed, shuffling phase information kept phase locking constant but fully abolished the phasic modulation of decision weighting (Figure 5B).

Transient changes in neural signals can resemble oscillations when analyzed using Fourier-based decompositions. To further test whether the observed fluctuations in decision weighting reflected a truly cyclic process, not just a transient change in broadband EEG signals, we first varied the temporal spread σ of the Gaussian envelope used to estimate delta phase and measured the temporal spread for which the effect of parietal delta phase on w_k was strongest at 500 ms following element k (see Experimental Procedures). This analysis identified an optimal temporal spread of four cycles—i.e., a full width at half maximum of 750 ms, indicating that the slow fluctuations in decision weighting spanned more than one delta cycle. Besides, time-frequency decompositions of transient changes in EEG signals typically show low-frequency specificity, spanning frequencies across multiple octaves. Here, by contrast, the phasic modulation of decision weighing was fully circumscribed to the delta range (Figure S5), consistent with a genuinely rhythmic process.

Finally, we re-estimated delta phase using a non-Fourier-based approach, namely, the Hilbert transform, and obtained the same phasic modulation of decision weighting. To do so, we band-pass-filtered single-trial EEG signals between 1 and 4 Hz and estimated the analytic phase of the EEG signals at each time point from 0 to 1,000 ms following element k at parietal electrodes (see Experimental Procedures). The preferred phase with respect to the decision weight w_k shifted linearly over time from 100 to 750 ms following element k—hence spanning more than one delta cycle and confirming that the phasic modulation of decision weighting is not due to a single transient change in EEG signals (Figure 5C). Besides, entering simultaneously previous (k−1), current (k), and next (k+1) elements as separate interaction terms showed overlapping

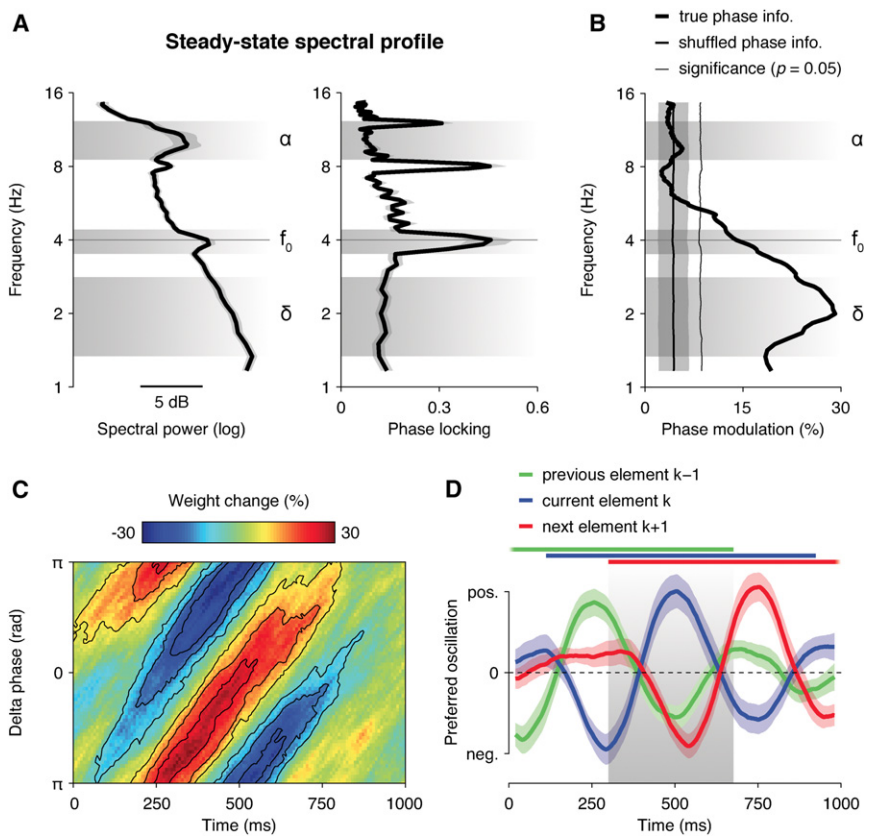

Figure 5. Oscillatory Properties of Slow Fluctuations in Decision Weighting

(A) Steady-state spectral power (left) and phase locking (right) across trials between 1 and 16 Hz, averaged across occipital and parietal electrodes, showing anticipated peaks at stimulation frequency f_0 and its higher harmonics but no peak in the delta band (1–4 Hz). Shaded error bars indicate SEM.

(B) Phase modulation of decision weight w_k at 500 ms following element k. The thick black line indicates modulation strength using the true phase information, and the thinner black line (mean ± standard deviation of the mean) using trial-shuffled phase information. The thin black line indicates the bootstrapped p = 0.05 significance threshold (two-tailed).

(C) Relationship between delta phase, estimated as the analytic phase of band-pass-filtered EEG signals between 1 and 4 Hz, and decision weight w_k between 0 and 1,000 ms following element k. The preferred delta phase with respect to decision weight w_k follows a damped delta oscillation at 2 Hz peaking around 500 ms following element k.

(D) Overlapping oscillations with opposite preferred phases for current (blue) versus previous (green) and next (red) elements. Shaded error bars indicate SEM. Thick horizontal lines indicate significant time windows ($p < 0.05$, two-tailed) for previous, current, and next elements, overlapping at 300–650 ms following element k.

influences of delta phase on the weighting of successive elements from 300 to 650 ms following element k ($p < 0.05$), with opposite preferred phases for current versus previous/next elements (Figure 5D).

Endogenous, Not Exogenous, Dynamics of Neural Encoding and Decision Weighting

Several features of the data strongly suggest that the phasic modulation of neural encoding and decision weighting was not occurring at a fixed subharmonic of the 4 Hz stimulation rate. Nevertheless, we sought to confirm that the time courses of neural encoding (Figure 2) and decision weighting (Figure 3) also reflected endogenous cortical dynamics, rather than being mainly driven by the stimulation frequency f_0.

To do so, we obtained additional EEG data from an independent group of 17 participants who performed the same categorization task at a different stimulation rate of 3 Hz (see Supplemental Information). We compared the estimated neural encoding and decision weighting time courses between these two data sets (Figures 6 and S6). At both stimulation rates, the peak latencies of neural encoding and decision weighting did not differ significantly (paired t test, both $p > 0.5$). And critically, we found no difference in peak latencies for neural encoding and decision weighting between the two stimulation rates (two-sample t test; neural encoding: 508 ± 20 ms at 4 Hz, 552 ± 22 ms at 3 Hz, $t_{30} = 1.4$, $p > 0.1$; decision weighting: 518 ± 12 ms at 4 Hz, 532 ± 34 ms at 3 Hz, $t_{30} < 1$, $p > 0.5$). Furthermore, while the neural encoding and decision weighting profiles for element k peaked around the onset of element k+2 at a stimulation rate of 4 Hz (t test against 500 ms; neural encoding: $t_{14} < 1$, $p > 0.5$; decision weighting: $t_{14} = 1.4$, $p > 0.1$), they peaked significantly earlier than the onset of element k+2 at 3 Hz (t test against 667 ms; neural encoding: $t_{16} = -5.1$, $p < 0.001$; decision weighting: $t_{16} = -4.0$, $p = 0.001$). The relative stability of peak latencies across stimulation frequencies confirms that the two profiles do not follow a fixed subharmonic of f_0.

Neural Encoding of the Integrated Evidence in Motor Beta-Band Activity

Previous noninvasive studies in humans have identified a different neural correlate of evidence accumulation, in the form of lateralized beta-band power (10–30 Hz) over the motor cortex preceding a left- or right-handed response (Donner et al., 2009). However, it remains unclear whether this neural signal contributes to the weighting of momentary evidence or rather reflects its downstream integration as a response preparation signal.

To arbitrate between these two possibilities, we carried out further analyses. First, we assessed the neural encoding of *response updates*—i.e., decision updates signed according to the stimulus-response mapping used by each participant, in lateralized beta-band power. In other words, we estimated the extent to which interhemispheric differences in beta-band activity (see Experimental Procedures) covaried with the

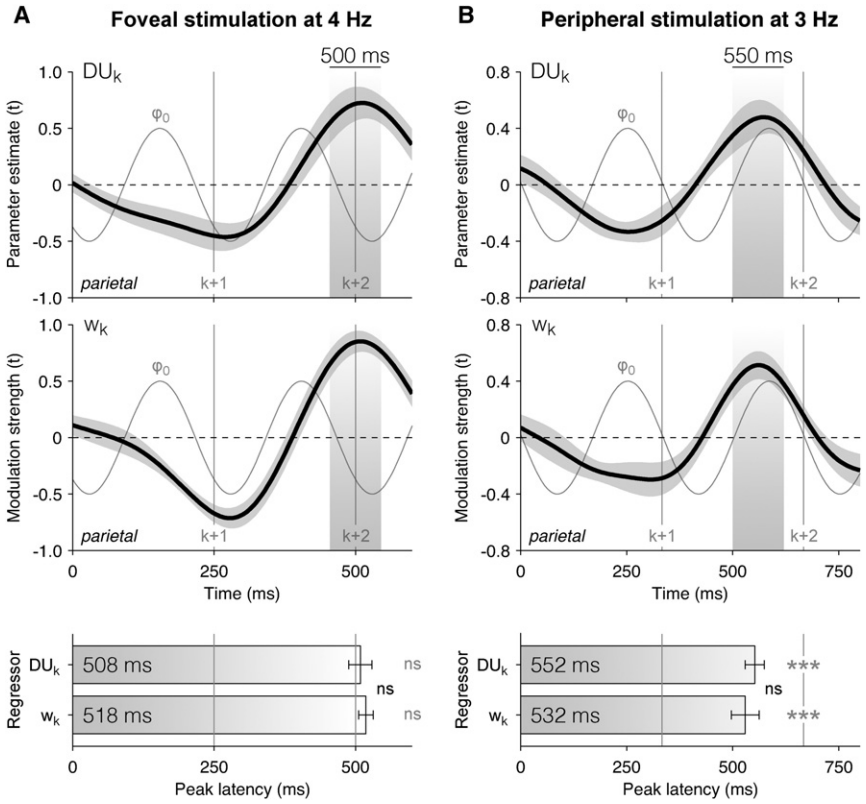

Figure 6. Preserved Neural Encoding and Decoding Profiles at Different Stimulation Rates

(A) Neural encoding and decoding profiles at a stimulation rate of 4 Hz. Upper panels: neural encoding (of decision update DU_k) and decoding (of decision weight w_k) profiles estimated from delta-band-filtered EEG signals (1–4 Hz) at parietal electrodes. Shaded areas highlight the positive encoding/decoding component peaking at 500 ms following element k. The thin gray line indicates the phase-locked oscillation φ_0 at the stimulation frequency. Shaded error bars indicate SEM. Lower panel: peak latencies of the positive encoding/decoding component. Error bars indicate SEM.

(B) Preserved neural encoding and decoding profiles obtained from an independent data set at a stimulation rate of 3 Hz. Same conventions as in (A). Note that the positive encoding/decoding components peak at different parts of the phase-locked oscillation φ_0 between the two stimulation frequencies. Significant latency difference at ***$p < 0.001$. ns, nonsignificant latency difference.

response update RU_k across trials at successive time samples following element k (Figure 7A). The neural encoding of RU_k in motor beta-band activity (10–30 Hz) ramped up gradually from 500 ms onward at central electrodes (500–750 ms; t test against zero, $t_{14} = 3.4$, $p < 0.01$), notably later than its encoding in broadband signals at parietal electrodes (Figure 2B). This sustained encoding of successive response updates in motor beta-band activity contrasts sharply with the transient encoding of successive decision updates observed in parietal broadband signals.

We then asked whether the neural encoding of RU_k in motor beta-band activity predicted the multiplicative decision weight w_k assigned to element k in the subsequent choice, or instead covaried with an additive change in response bias—i.e., the probability of a left- or right-handed response irrespective of element k (see Experimental Procedures). To this end, we again related trial-to-trial variability in neural encoding to variability in choice. But in this psychophysiological analysis, choice was predicted via two separate modulatory terms: (1) the interaction between each decision update DU_k and the corresponding encoding residuals $r_{k,t}$ at time t (parameterized by $w_{k,t}$), and (2) the main effect of encoding residuals $r_{k,t}$ at time t (parameterized by $b_{k,t}$):

$$P(\text{cardinal}) = \Phi\left[b + \sum_{k=1}^{8} w_k \cdot DU_k + \sum_{k=1}^{8} b_{k,t} \cdot r_{k,t} + w_{k,t} \cdot DU_k \times r_{k,t}\right].$$

Consistent with a response preparation signal, we found that encoding residuals following element k predicted $b_{k,t}$ (500–750 ms, t test against zero, $t_{14} = 6.7$, $p < 0.001$) but not $w_{k,t}$ ($t_{14} = -1.6$, $p > 0.1$), indicating that motor beta-band activity had an additive, not a multiplicative, influence on decision making (Figure 7B). In accordance with this interpretation, the strength of this psychophysiological modulation increased parametrically across successive elements (repeated-measures ANOVA, $F_{7,98} = 18.6$, $p < 0.001$)—i.e., with temporal proximity from the motor response. This is to be expected from a response preparation signal driven by large temporal fluctuations in sensory input (Yang and Shadlen, 2007).

We carried out additional analyses locked to the onset of the response period, which all confirmed that motor beta-band activity behaved as a response preparation signal (Figure S7): (1) the neural encoding of the sum of response updates distinguished correct choices from errors from more than 500 ms before the onset of the response period (paired t test, $t_{14} = 4.8$, $p < 0.001$); (2) the neural decoding of choice (i.e., left- versus right-handed response) showed similar predictive profiles preceding correct choices and errors (see Supplemental Information); and (3) the between-element variability in neural encoding of response updates correlated positively with the between-element weighting profile estimated behaviorally ($r = +0.44 \pm 0.10$, t test against zero, $t_{14} = 4.4$, $p < 0.001$).

Finally, we assessed whether the neural encoding of DU_k in motor beta-band activity also fluctuated rhythmically according to the phase of parietal delta oscillations (Figure 7C), and found that it followed the same phase relationship as its earlier encoding in broadband parietal signals (Rayleigh test, $r_{14} = 0.50$, $p < 0.01$). This phase dependency suggests that motor beta-band activity reflects a computation that occurs downstream from the weighting of momentary evidence according to the phase of parietal delta oscillations.

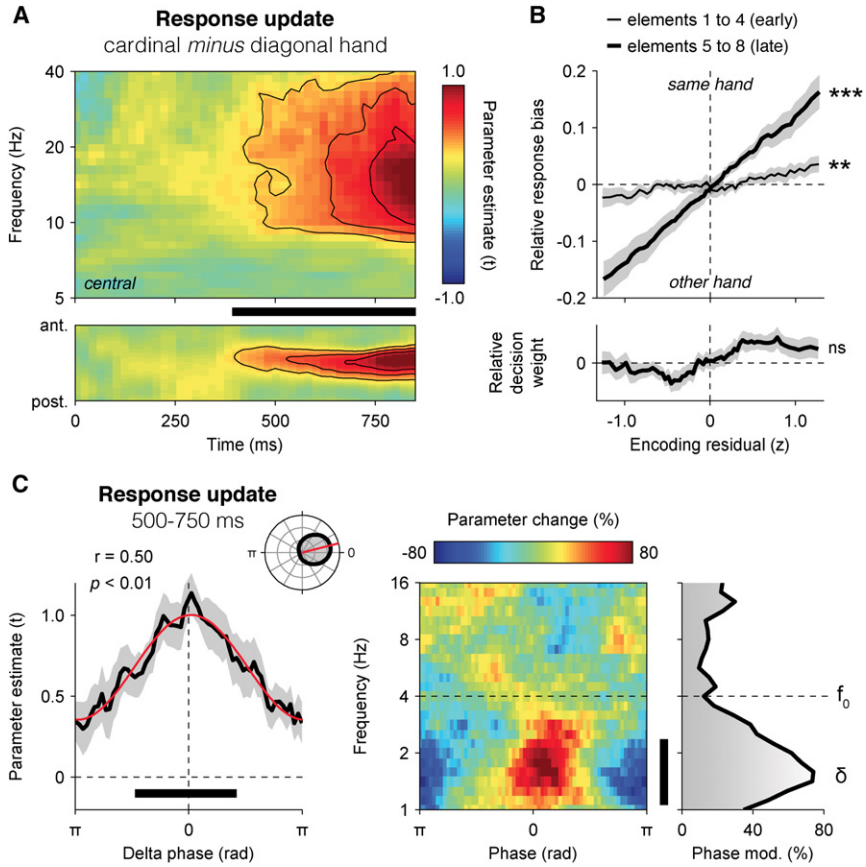

Figure 7. Neural Encoding of the Running Decision Variable in Motor Beta-Band Activity

(A) Neural encoding of response update RU_k in motor beta-band activity (10–30 Hz), expressed as parameter estimate in t units. Upper panel: encoding time-frequency profile at motor electrodes (above) and following the anteroposterior gradient (below). The thick black bar indicates cluster-level significance at $p < 0.001$.

(B) Relationship between encoding residuals in motor beta-band activity and the relative response bias (upper panel) or decision weight (lower panel) at 500–750 ms following early elements 1–4 (thin line) and late elements 5–8 (thick line). Shaded error bars indicate SEM. Significant correlation at $^{**}p < 0.01$ and $^{***}p < 0.001$; ns, nonsignificant correlation.

(C) Phase-dependent fluctuations in the neural encoding of response update RU_k in motor beta-band activity (10–30 Hz). Left panel: relationship between the phase of parietal delta oscillations at 500 ms following element k and the encoding of RU_k in motor beta-band activity at 500–750 ms. Right panel: relationship between the phase of parietal EEG oscillations from 1 to 16 Hz at 500 ms following element k and the neural encoding of response update RU_k in motor beta-band activity. Same conventions as in Figure 4.

DISCUSSION

Together, these findings chart the electrophysiological substrates of the sensorimotor cascade whereby successive samples of sensory evidence are processed from lower to higher levels, integrated, and converted into an appropriate response. By linking trial-to-trial fluctuations in neural signals to variability in choice, these findings draw a clear distinction between the computations performed by two neural mechanisms during categorical decision making. First, momentary evidence undergoes a *multiplicative* weighting according to the phase of ongoing delta oscillations (1–3 Hz) overlying human parietal cortex. Subsequently, lateralized beta-band activity (10–30 Hz) over the motor cortex integrates the weighted evidence in an *additive* fashion, consistent with the formation of a decision variable. Categorical choices are thus preceded by discrete central and motor stages, both of which follow an early perceptual stage confined to early visual cortex. These findings thus call into question the widely held view that evidence accumulation is indistinguishable from the gradual engagement of a response effector—in other words, that the neural encoding of decision-relevant evidence reduces to a preparatory signal that precedes motor output (Shadlen and Newsome, 2001; Roitman and Shadlen, 2002; Gold and Shadlen, 2003, 2007).

Moreover, while current decision-theoretic models describe evidence accumulation as a linear process whereby successive samples of evidence are integrated at a constant rate over hundreds of milliseconds (Ratcliff and Smith, 2004; Gold and Shadlen, 2007), we show that both the encoding of momentary evidence in the human EEG and its impact on decision making fluctuate in a rhythmic fashion: samples of evidence processed in the preferred delta cycle are overweighted and followed by underweighted samples processed in the opposite cycle 250 ms later. The timing of this push-pull pattern of decision weighting forges a link between a recent decision-making literature and classic psychological accounts of capacity limits in human perception (Pashler, 1984; Raymond et al., 1992; Marois and Ivanoff, 2005). Our findings suggest that the serial attentional bottleneck identified as responsible for refractory phenomena such as the attentional blink (Sergent et al., 2005; Sigman and Dehaene, 2008; Tombu et al., 2011) might impose a general sampling constraint on decision making over several hundreds of milliseconds. This finding points to a previously unaccounted-for source of variability in human decisions and imposes an important limitation on decision-theoretic models—such as diffusion or "race" models—in which successive samples are totted up linearly toward a decision bound, suggesting that they are a suitable descriptor of sensorimotor decisions only when occurring over very short timescales.

Our findings invite obvious parallels with a literature describing how a second target stimulus (T2) is often missed if it occurs shortly after a first target stimulus (T1), not least because the attentional blink is maximal when T1 and T2 are separated by approximately 250 ms, or "lag-2" (Raymond et al., 1992)—i.e., the peak-to-trough latency with respect to a 2 Hz cycle. Even more notably, the finding that decision weighting fluctuates

rhythmically at approximately 2 Hz is consistent with a related finding, namely, that when T2 follows T1 at a very short latency (e.g., 125 ms) it is less likely to be missed, a phenomenon known as "lag-1 sparing" (Chun and Potter, 1995). Assuming that the phase of ongoing delta oscillations is at least partially reset by the occurrence of T1, an unexpected T2 occurring at 125 ms post-T1 (lag-1) will fall in the waning portion of the delta cycle, whereas a T2 occurring at 250 ms (lag-2) will fall close to its nadir, such that T2 is more likely to be processed (and hence detected) at lag-1 than at lag-2. Finally, subliminal effects of "blinked" stimuli on subsequent decisions have been interpreted as indicating a preserved perceptual processing of blinked stimuli (Dehaene et al., 2006). Accordingly, we find that delta phase has a much stronger modulatory influence on the encoding of decision-relevant information than that of perceptual information.

However, our findings also offer an explanation for a phenomenon that has long puzzled researchers interested in modeling decision latencies—that serial models of the decision process (such as diffusion-to-bound models) can only account for the relative speeds of errors and correct choices if drift rate (i.e., the rate of evidence accumulation) is allowed to vary across trials. Varying drift rate randomly across successive trials allows different admixtures of trials with high and low drift rates to drive correct and incorrect choices, leading to the widely observed phenomenon that decision latencies for errors typically exceed those for correct choices (Ratcliff and Rouder, 1998). Even within each trial, the gradual buildup of neuronal firing rates in sensorimotor cortex is known to vary stochastically in a fashion that predicts the dynamics of the eventual movement (Hanes and Schall, 1996). Our findings suggest a neurophysiological explanation for these two phenomena—that the rate of evidence accumulation varies within the course of a single trial according to the phase of ongoing slow cortical oscillations.

Measuring the temporal spread of this cyclic modulation of information processing revealed that it lasted for several delta cycles, and was thus not simply a transient, discrete activity evoked by each element. Nevertheless, the influence of parietal delta phase on decision weighting tapered off quite rapidly, indicating that this rhythmic mechanism is not a rigid oscillatory mechanism but rather can be flexibly aligned to account for the changing demands of information processing—e.g., become entrained to the onset of relevant stimuli when they are presented at predictable times at delta-band (<3 Hz) stimulation frequencies (Lakatos et al., 2008; Schroeder and Lakatos, 2009; Stefanics et al., 2010). However, the strongest competition was observed between a given element and its immediate neighbors—within each delta cycle—as expected if successive samples of information were competing to pass through a serial processing bottleneck.

Finally, these findings shed light on the role of slow cortical oscillations in sensory selection (Lakatos et al., 2008; Schroeder and Lakatos, 2009; Stefanics et al., 2010). Previous research has demonstrated that the encoding of sensory information depends on the phase of delta oscillations in sensory cortex, but because stimulation occurred in the delta band, it is hard to tell whether this modulation was dependent on being driven exogenously (entrained) by the *external* stimulation rhythm. Here we show that the neural encoding of both perceptual and categorical information in the human EEG was modulated by an *internal* rhythm distinct from the stimulation frequency. This finding demonstrates unambiguously that the selection of perceptual and categorical information is dependent on endogenous delta oscillations, not on the entrainment of neural oscillations to any stimulation frequency. Moreover, although the source of observed neural activity is hard to pinpoint with scalp EEG recordings, we observed the encoding and decoding of decision information relatively diffusely across the scalp, with maxima over the parietal cortex, suggesting that slow cortical oscillations contribute to information processing beyond primary sensory cortices.

One possibility is that this rhythmic sampling mechanism may have evolved to ensure that the neural processing of currently available information is not corrupted by potentially distracting information arriving in its immediate wake. It might also be that slow reverberatory activity may inject stochasticity into a neural circuitry that, coupled with attractor dynamics, helps mediate the tradeoff between exploratory and exploitative behavior (Soltani and Wang, 2008, 2010). Interestingly, unlike the neural encoding of decision-relevant information, which depended exclusively on the phase of delta oscillations, the gain of visual responses also followed the phase of faster cortical rhythms around 8 Hz. This finding is consistent with recent reports that evoked visual responses and signal detectability depend on the phase of EEG oscillations in this frequency range in humans (Busch et al., 2009; Wyart and Sergent, 2009; Scheeringa et al., 2011). The particular frequency of fluctuations in neural excitability may reflect the predominant time constants of synaptic activity in the corresponding cortical area (Wang, 2010; Bernacchia et al., 2011).

To conclude, we found that during extended categorical decisions, the rate of evidence accumulation fluctuates over time, in a fashion that can be predicted from the ongoing phase of slow EEG oscillations in the delta band (1–3 Hz) overlying human parietal cortex. Large-scale delta oscillations thus appear as an excellent candidate substrate for the serial attentional bottleneck known to give rise to a range of cognitive phenomena such as the attentional blink and the psychological refractory period. These findings suggest that slow rhythmic changes in cortical excitability form a tight temporal constraint on sequential information processing.

EXPERIMENTAL PROCEDURES

Participants

Sixteen students were recruited from the University of Oxford (age range: 18–25 years). All had normal or corrected-to-normal vision, and reported no history of neurologic or psychiatric disorders. They provided written consent before the experiment and received £30 in compensation for their participation, in addition to bonuses depending on their categorization performance (approximately £5). The experiment followed local ethics guidelines. The data from one participant were not included because of excessive eye blinks.

Stimuli

Visual stimuli were presented using the Psychophysics-3 Toolbox (Brainard, 1997; Pelli, 1997) and additional custom scripts written for MATLAB (The Mathworks). The display CRT monitor had a resolution of 1,024 × 768 pixels, a refresh rate of 60 Hz, and was gamma corrected using a decoding exponent

of 2.2. Participants viewed the stimuli from a distance of approximately 80 cm in a darkened room.

Each trial comprised a sequence of eight centrally presented Gabor patterns presented every 250 ms (4 Hz), preceded by two visual masks and followed by one visual mask presented at the same frequency. All Gabor patterns had identical parameters (contrast: 50%; diameter: four degrees of visual angle; spatial frequency: two cycles per degree of visual angle; Gaussian envelope SD: one degree of visual angle), except for their tilt. Masks were created from the linear superposition of the four cardinal and diagonal Gabor patterns. Each stimulus was presented on the screen for 233.3 ms (14 frames) and followed by a blank period of 16.7 ms (1 frame) to avoid visual "tearing" artifacts across successive elements, thus resulting in a stimulus onset asynchrony of 250 ms (i.e., 4 Hz).

Task Design

In each trial, the tilt of each Gabor pattern (or element) was drawn randomly from a probability density function whose generating parameters were titrated for each participant prior to the experiment (see below). Across trials, the tilt of each Gabor pattern was distributed uniformly. Following each stream, participants reported whether, on average, the tilt of the eight elements fell closer to the cardinal or diagonal axes. Positive or negative feedback was provided on the basis of the average of eight decision values corresponding to the angular distance between the tilt of each element to the cardinal or diagonal axes, normalized between −1 (diagonal) and +1 (cardinal). The unsigned decision value, or *decision update*, associated with each element was also distributed uniformly. Trials corresponding to a negative average decision value were associated with the diagonal response, while those corresponding to a positive average decision value were associated with the cardinal response.

Participants responded by pressing either of the two Ctrl keys of a standard keyboard with their left or right index finger, using a cardinal/diagonal response mapping (e.g., cardinal: left; diagonal: right) fully counterbalanced across participants. Auditory feedback was given at the end of each trial—250 ms following each response—depending on the agreement between the response and the sign of the average decision value (or category-level average) across the eight elements. Increasing pairs of tones (440/880 Hz) followed correct responses, whereas decreasing ones (880/440 Hz) followed errors.

Prior to the experiment, each participant undertook a short practice session followed by a titration session during which his or her psychophysical threshold—i.e., the unsigned category-level average corresponding to a categorization accuracy of 75%—was estimated using an adaptive staircase procedure (Kaernbach, 1991). This threshold estimate was then used to determine five evenly spaced levels of category-level average, from a diagonal to a cardinal average, split into three difficulty levels. Easy cardinal/diagonal trials (1/3 of all trials) corresponded to a categorization sensitivity d′ of 2.12 ± 0.18 (mean ± SEM), whereas difficult cardinal/diagonal trials (1/3 of all trials) corresponded to a d′ of 1.00 ± 0.09. Neutral trials (1/3 of all trials) corresponded to a null category-level average, and were associated with a pseudorandom feedback, positive on 60% of neutral trials. The experiment consisted of 672 trials, divided into seven sessions of 96 trials.

After each session, participants were presented with a wheel of fortune that randomly selected one trial from the block; participants won an additional £1 bonus if their response on that trial was correct. The titration procedure ensured that participants typically won £5 in additional bonuses across the seven experimental sessions.

EEG Acquisition and Preprocessing

A Neuroscan system with SynAmps-2 digital amplifiers was used to record EEG signals from 32 Ag/AgCl electrodes located at FP1, FPz, FP2, F7, F3, Fz, F4, F8, FT7, FC3, FCz, FC4, FT8, T7, C3, Cz, C4, T8, TP7, CP3, CPz, CP4, TP8, P7, P3, Pz, P4, P8, POz, O1, Oz, and O2, plus four additional electrodes used in a bipolar montage as horizontal and vertical electro-oculograms (EOGs) and two electrodes located at the mastoids used as reference. All electrode impedances were kept below 50 kΩ. EEG signals were recorded at a sampling rate of 1,000 Hz and high-pass filtered online at 0.1 Hz.

Preprocessing was carried out using the EEGLAB toolbox for MATLAB (Delorme and Makeig, 2004). The data were downsampled to 250 Hz, band-pass-filtered between 1 and 40 Hz, and then epoched from 500 ms before the onset of the first premask to 1 s following the offset of the postmask (i.e., 1 s following the onset of the response period). We visually inspected these epochs (1) to remove trials containing nonstereotypical artifacts (such as transient muscular activity) and (2) to identify "bad" electrodes showing frequent amplifier "jumps" or other electrical artifacts (e.g., spikes), which were interpolated to the weighted average of neighboring electrodes. A maximum of one electrode was identified as bad per participant, and only for 3 of the 15 recorded participants.

Independent component analysis (ICA) was then performed on the epoched data as implemented in EEGLAB—excluding the EOG, reference, and interpolated electrodes from the analysis—and ICA components were visually inspected to reject the ones capturing stereotypical artifacts (in particular eye blinks and sustained high-frequency noise). Finally, single epochs were reinspected visually to ensure that no artifact remained. Rejected trials were excluded from all further analyses, resulting in an average of 565 ± 15 trials per participant (mean ± SEM).

Steady-state frequency spectra were estimated using a standard Fourier transform from the onset of the first element (i.e., following the two premasks) until the offset of the last element (i.e., preceding the postmask). Frequency power was defined as the average square amplitude of complex Fourier components, whereas phase locking was defined as the length of the vector average of single-trial phase estimates.

Time-frequency analyses were carried out using the FieldTrip toolbox for MATLAB (Oostenveld et al., 2011). The phase of slow EEG oscillations was estimated using either a wavelet transform (Morlet wavelets, frequency range: 1–16 Hz, four cycles per window) or a Hilbert transform applied to band-pass-filtered EEG signals in the delta band (1–4 Hz). While both methods provided time-resolved estimates of EEG phase at the single-trial level, the Hilbert transform did not make any assumption regarding the sinusoidal nature of narrow-band EEG signals. The spectral power of beta-band EEG oscillations (>10 Hz) was estimated using a "multitapering" time-frequency transform (Mitra and Pesaran, 1999; Pesaran et al., 2002), as implemented in FieldTrip (Slepian tapers, frequency range: 5–40 Hz, five cycles and three tapers per window). The purpose of this multitapering approach is to obtain more precise power estimates by smoothing across frequencies. Note that both time-frequency transforms use a constant number of cycles across frequencies, hence a time window whose duration decreases inversely with increasing frequency.

For simplicity, we report statistical tests on EEG data averaged across electrode sites. Occipital electrodes correspond to electrodes O1, Oz, and O2. Parietal electrodes correspond to electrodes P3, Pz, P4, and POz. Central/motor electrodes correspond to electrodes C3 and C4, analyzed as their difference to calculate an interhemispheric asymmetry index.

EEG Analysis—Neural Encoding of Parametric Information

We regressed single-trial EEG signals against several parametric quantities associated with individual elements at successive time samples following the onset of the corresponding element. These analyses were carried out separately for each of the eight elements in the stream, averaged across elements, and finally averaged across participants to produce a group-level grand average.

For each element k, a general linear regression model was used in which we included the perceptual update PU_k and the decision update DU_k as two parametric regressors to predict the trial-to-trial variability in EEG signals at a given time t following element k. This parametric regression was done separately at successive times from 0 to 600 ms following element k. The time course of the corresponding parameter estimates—i.e., the normalized best-fitting regression coefficients, expressed in between-trial t units—measured the sensitivity of single-trial EEG signals to perceptual and decision updates. Because these time courses are time series of the between-trial correlation between the EEG and element k, we refer to them as describing the neural *encoding* of perceptual/decision updates provided by element k.

Baselining for this regression-based analysis was performed by decorrelating the EEG signal at each electrode and each time following the onset of element k from trial-to-trial variability in the EEG signal at the last time sample before the onset of element k. The rationale behind this baselining strategy is that trial-to-trial variability in the EEG signal before the onset of

element k could not be related to the encoding of element k. Applying this baseline or not did not change the pattern or overall significance of the observed effects.

A comparable approach was adopted to assess how response-mapped decision updates were encoded in interhemispheric beta-band activity (10–30 Hz) at central electrodes. For each participant, we calculated single-trial spectral power from 5 to 40 Hz at electrodes C3 (overlying the left motor cortex) and C4 (overlying the right motor cortex) and subtracted spectral power between these electrodes, C3 minus C4 or C4 minus C3, depending on the cardinal/diagonal response mapping used for each participant; the motor electrode associated with "cardinal" responses (C4 if the participant responded "cardinal" with his or her left index finger, or C3 otherwise) was counted positively, whereas the motor electrode associated with "diagonal" responses was counted negatively.

EEG Analysis—Psychophysiological Interaction Analysis

We used an approach analogous to a psychophysiological interaction analysis (Friston et al., 1997) to assess the relationship between the encoding of DU_k and the decision weight w_k assigned to that element in the subsequent categorical choice. We refer to this analysis scheme as a neural *decoding* approach because it quantifies how trial-to-trial variability in the neural encoding of element k in the EEG—i.e., residuals from the *encoding* regression described above—covaried with its decision weighting across trials.

To do so, we quantified whether and how much trial-to-trial fluctuations in EEG signals exerted a *modulatory* influence on the relationship between the eight decision updates and choice via multivariate parametric regression. In other words, we determined whether EEG-informed regressions of choice led to a significant increase in prediction accuracy. This type of approach is often called "psychophysiological," because it assesses how trial-to-trial variability in the EEG (i.e., a *physiological* variable) modulates the relationship between decision updates and the subsequent categorical choice (i.e., a *psychological* variable).

Within the general linear model framework, a psychophysiological modulation can take either of two forms: (1) a *multiplicative* modulation, or interaction, corresponding to a modulation of the decision weight w_k assigned to one (or several) of the eight elements in the subsequent choice; or (2) an *additive* modulation, corresponding to a modulation of response bias—i.e., the probability of a "cardinal" or "diagonal" response irrespective of element k. In all psychophysiological analyses, choice was thus predicted via two separate modulatory terms on top of the weighted decision updates $w_k \cdot DU_k$ and the overall response bias *b* entered as offset terms in a multivariate parametric regression: (1) the interaction between each decision update DU_k and the corresponding EEG encoding residuals $r_{k,t}$, and (2) the main effect of EEG encoding residuals $r_{k,t}$. Importantly, psychophysiological analyses assume that EEG encoding residuals covary linearly either with the *multiplicative* decision weight assigned to successive elements or with the *additive* response bias in favor of one of the two categories.

This psychophysiological regression provided parameter estimates for the two modulatory terms: (1) the strength of the *multiplicative* modulation of the decision weight assigned to element k, and (2) the strength of the *additive* modulation of response bias. A nonzero parameter estimate for the *multiplicative* modulation term indicates that the physiological signal modulates the contribution of the corresponding decision update on choice. By contrast, a nonzero parameter estimate for the *additive* modulation term indicates that the physiological signal biases responses toward either the cardinal or diagonal category irrespective of the corresponding decision update.

We first used this psychophysiological modulatory approach to investigate whether trial-to-trial variability in the neural encoding of DU_k at parietal electrodes modulated the decision weight w_k assigned to element k in the eventual choice. To address this question, we applied the approach described above by taking as physiological variable the trial-to-trial encoding residuals from DU_k at parietal electrodes, calculated at each electrode and each time from 0 to 600 ms following the onset of element k. We then extended this analysis to temporally adjacent elements in the stream by including not only the interaction between encoding residuals from element k and DU_k but also the interaction between encoding residuals from element k and adjacent decision updates DU_{k-1} and DU_{k+1}.

We also applied this psychophysiological modulatory approach to phase φ of EEG oscillations, a circular quantity defined between $-\pi$ and π. We took into account the notion that φ is a complex-valued physiological variable by performing separate real-valued psychophysiological analyses for $\sin(\varphi)$ and for $\cos(\varphi)$, and by recovering the strength of the modulation and the corresponding preferred phase using the quadratic pair relationship.

When assessing how trial-to-trial fluctuations in lateralized beta-band activity at motor electrodes influenced the subsequent choice, we acknowledged that beta-band activity did not encode successive decision updates discretely and transiently as observed in broadband signals at parietal electrodes, but rather in a cumulative ramping-up fashion, and used the encoding residuals from the running decision variable—i.e., the cumulative sum of individual updates up to element k—rather than the encoding residuals from DU_k in isolation.

EEG Analysis—Statistical Procedures

The neural encoding and decoding analyses described above were performed separately for each participant and each element. At the group level, we used standard parametric tests (e.g., paired t tests and repeated-measures ANOVAs) to assess the statistical significance of observed effects across the group. The type 1 error rate arising from multiple comparisons was controlled for using nonparametric cluster-level statistics (Maris and Oostenveld, 2007) computed across electrodes, time samples, and frequencies.

SUPPLEMENTAL INFORMATION

Supplemental Information includes seven figures, Supplemental Results, and Supplemental Experimental Procedures and can be found with this article online at http://dx.doi.org/10.1016/j.neuron.2012.09.015.

ACKNOWLEDGMENTS

We would like to thank Nick Yeung and Kia Nobre for providing access to their EEG equipment, Nick Myers for assistance with EEG acquisition, and Tim Behrens, Etienne Koechlin, Benjamin Morillon, and Mark Stokes for useful suggestions and comments. V.W. is supported by a postdoctoral research grant from the Fyssen Foundation.

Accepted: September 4, 2012
Published: November 21, 2012

REFERENCES

Bernacchia, A., Seo, H., Lee, D., and Wang, X.J. (2011). A reservoir of time constants for memory traces in cortical neurons. Nat. Neurosci. *14*, 366–372.

Bogacz, R., Brown, E., Moehlis, J., Holmes, P., and Cohen, J.D. (2006). The physics of optimal decision making: a formal analysis of models of performance in two-alternative forced-choice tasks. Psychol. Rev. *113*, 700–765.

Brainard, D.H. (1997). The Psychophysics Toolbox. Spat. Vis. *10*, 433–436.

Busch, N.A., and VanRullen, R. (2010). Spontaneous EEG oscillations reveal periodic sampling of visual attention. Proc. Natl. Acad. Sci. USA *107*, 16048–16053.

Busch, N.A., Dubois, J., and VanRullen, R. (2009). The phase of ongoing EEG oscillations predicts visual perception. J. Neurosci. *29*, 7869–7876.

Chun, M.M., and Potter, M.C. (1995). A two-stage model for multiple target detection in rapid serial visual presentation. J. Exp. Psychol. Hum. Percept. Perform. *21*, 109–127.

Dehaene, S., Changeux, J.P., Naccache, L., Sackur, J., and Sergent, C. (2006). Conscious, preconscious, and subliminal processing: a testable taxonomy. Trends Cogn. Sci. *10*, 204–211.

Delorme, A., and Makeig, S. (2004). EEGLAB: an open source toolbox for analysis of single-trial EEG dynamics including independent component analysis. J. Neurosci. Methods *134*, 9–21.

Donner, T.H., Siegel, M., Fries, P., and Engel, A.K. (2009). Buildup of choice-predictive activity in human motor cortex during perceptual decision making. Curr. Biol. *19*, 1581–1585.

Friston, K.J., Buechel, C., Fink, G.R., Morris, J., Rolls, E., and Dolan, R.J. (1997). Psychophysiological and modulatory interactions in neuroimaging. Neuroimage *6*, 218–229.

Gold, J.I., and Shadlen, M.N. (2003). The influence of behavioral context on the representation of a perceptual decision in developing oculomotor commands. J. Neurosci. *23*, 632–651.

Gold, J.I., and Shadlen, M.N. (2007). The neural basis of decision making. Annu. Rev. Neurosci. *30*, 535–574.

Hanes, D.P., and Schall, J.D. (1996). Neural control of voluntary movement initiation. Science *274*, 427–430.

Kaernbach, C. (1991). Simple adaptive testing with the weighted up-down method. Percept. Psychophys. *49*, 227–229.

Lakatos, P., Karmos, G., Mehta, A.D., Ulbert, I., and Schroeder, C.E. (2008). Entrainment of neuronal oscillations as a mechanism of attentional selection. Science *320*, 110–113.

Link, S.W. (1975). The relative judgment theory of two choice response time. J. Math. Psychol. *12*, 114–135.

Maris, E., and Oostenveld, R. (2007). Nonparametric statistical testing of EEG- and MEG-data. J. Neurosci. Methods *164*, 177–190.

Marois, R., and Ivanoff, J. (2005). Capacity limits of information processing in the brain. Trends Cogn. Sci. *9*, 296–305.

Mitra, P.P., and Pesaran, B. (1999). Analysis of dynamic brain imaging data. Biophys. J. *76*, 691–708.

Oostenveld, R., Fries, P., Maris, E., and Schoffelen, J.M. (2011). FieldTrip: open source software for advanced analysis of MEG, EEG, and invasive electrophysiological data. Comput. Intell. Neurosci. *2011*, 156869.

Pashler, H. (1984). Processing stages in overlapping tasks: evidence for a central bottleneck. J. Exp. Psychol. Hum. Percept. Perform. *10*, 358–377.

Pelli, D.G. (1997). The VideoToolbox software for visual psychophysics: transforming numbers into movies. Spat. Vis. *10*, 437–442.

Pesaran, B., Pezaris, J.S., Sahani, M., Mitra, P.P., and Andersen, R.A. (2002). Temporal structure in neuronal activity during working memory in macaque parietal cortex. Nat. Neurosci. *5*, 805–811.

Ratcliff, R., and Rouder, J.N. (1998). Modeling response times for two-choice decisions. Psychol. Sci. *9*, 347–356.

Ratcliff, R., and Smith, P.L. (2004). A comparison of sequential sampling models for two-choice reaction time. Psychol. Rev. *111*, 333–367.

Raymond, J.E., Shapiro, K.L., and Arnell, K.M. (1992). Temporary suppression of visual processing in an RSVP task: an attentional blink? J. Exp. Psychol. Hum. Percept. Perform. *18*, 849–860.

Roitman, J.D., and Shadlen, M.N. (2002). Response of neurons in the lateral intraparietal area during a combined visual discrimination reaction time task. J. Neurosci. *22*, 9475–9489.

Scheeringa, R., Mazaheri, A., Bojak, I., Norris, D.G., and Kleinschmidt, A. (2011). Modulation of visually evoked cortical fMRI responses by phase of ongoing occipital alpha oscillations. J. Neurosci. *31*, 3813–3820.

Schroeder, C.E., and Lakatos, P. (2009). Low-frequency neuronal oscillations as instruments of sensory selection. Trends Neurosci. *32*, 9–18.

Sergent, C., Baillet, S., and Dehaene, S. (2005). Timing of the brain events underlying access to consciousness during the attentional blink. Nat. Neurosci. *8*, 1391–1400.

Shadlen, M.N., and Newsome, W.T. (2001). Neural basis of a perceptual decision in the parietal cortex (area LIP) of the rhesus monkey. J. Neurophysiol. *86*, 1916–1936.

Sigman, M., and Dehaene, S. (2008). Brain mechanisms of serial and parallel processing during dual-task performance. J. Neurosci. *28*, 7585–7598.

Soltani, A., and Wang, X.J. (2008). From biophysics to cognition: reward-dependent adaptive choice behavior. Curr. Opin. Neurobiol. *18*, 209–216.

Soltani, A., and Wang, X.J. (2010). Synaptic computation underlying probabilistic inference. Nat. Neurosci. *13*, 112–119.

Stefanics, G., Hangya, B., Hernádi, I., Winkler, I., Lakatos, P., and Ulbert, I. (2010). Phase entrainment of human delta oscillations can mediate the effects of expectation on reaction speed. J. Neurosci. *30*, 13578–13585.

Tombu, M.N., Asplund, C.L., Dux, P.E., Godwin, D., Martin, J.W., and Marois, R. (2011). A unified attentional bottleneck in the human brain. Proc. Natl. Acad. Sci. USA *108*, 13426–13431.

VanRullen, R., and Koch, C. (2003). Is perception discrete or continuous? Trends Cogn. Sci. *7*, 207–213.

Wald, A., and Wolfowitz, J. (1949). Bayes solutions of sequential decision problems. Proc. Natl. Acad. Sci. USA *35*, 99–102.

Wang, X.J. (2010). Neurophysiological and computational principles of cortical rhythms in cognition. Physiol. Rev. *90*, 1195–1268.

Wyart, V., and Sergent, C. (2009). The phase of ongoing EEG oscillations uncovers the fine temporal structure of conscious perception. J. Neurosci. *29*, 12839–12841.

Yang, T., and Shadlen, M.N. (2007). Probabilistic reasoning by neurons. Nature *447*, 1075–1080.